The Interannual Variability of the Haines Index over North America

LEJIANG YU

Applied Hydrometeorological Research Institute, Nanjing University of Information Science and Technology, Nanjing, China

SHIYUAN ZHONG

Department of Geography, and Center for Global Change and Earth Observations, Michigan State University, East Lansing, Michigan

XINDI BIAN, WARREN E. HEILMAN, AND JOSEPH J. CHARNEY

Northern Research Station, Forest Service, U.S. Department of Agriculture, East Lansing, Michigan

(Manuscript received 20 February 2013, in final form 14 June 2013)

ABSTRACT

The Haines index (HI) is a fire-weather index that is widely used as an indicator of the potential for dry, low-static-stability air in the lower atmosphere to contribute to erratic fire behavior or large fire growth. This study examines the interannual variability of HI over North America and its relationship to indicators of large-scale circulation anomalies. The results show that the first three HI empirical orthogonal function modes are related respectively to El Niño–Southern Oscillation (ENSO), the Arctic Oscillation (AO), and the interdecadal sea surface temperature variation over the tropical Pacific Ocean. During the negative ENSO phase, an anomalous ridge (trough) is evident over the western (eastern) United States, with warm/dry weather and more days with high HI values in the western and southeastern United States. During the negative phase of the AO, an anomalous trough is found over the western United States, with wet/cool weather and fewer days with high HI, while an anomalous ridge occurs over the southern United States–northern Mexico, with an increase in the number of days with high HI. After the early 1990s, the subtropical high over the eastern Pacific Ocean and the Bermuda high were strengthened by a wave train that was excited over the tropical western Pacific Ocean and resulted in warm/dry conditions over the southwestern United States and western Mexico and wet weather in the southeastern United States. The above conditions are reversed during the positive phase of ENSO and AO and before the early 1990s.

1. Introduction

The Haines index (HI), also called a lower-atmospheric severity index (Haines 1988), is a tool used by fire-weather forecasters and fire managers to assess the potential for conditions in the lower troposphere to influence the evolution of a wildland fire. The HI depends upon static stability (factor A) and dewpoint depression (factor B) in a predefined atmospheric layer and combines the two factors into a single number that indicates the potential for an existing fire to exhibit erratic fire behavior or to grow large. Each factor can have a value of 1, 2, or 3 according to predetermined thresholds, and HI is calculated by summing the two factors. An HI of 2 or 3 indicates

a low potential for fires to exhibit erratic behavior or to grow large, and a 6 indicates a very high potential (Haines 1988). A detailed description of HI and how it is calculated can be found in Haines (1988).

Although developed with a limited dataset in the United States, HI has been widely used for operational fire-weather forecasts in regions of the United States, Canada, and Australia. Several studies have shown a positive correlation between HI and observed fire activity. For example, Bally (1995) showed that a large percentage of fires in Tasmania, Australia, occurred on days with an HI ≥ 5. Werth and Ochoa (1993) showed that the index performs well at pinpointing the time of the most explosive fire growth for two wildfire cases in Idaho and that on a seasonal scale the index is useful in determining when the most acreage will be lost to wildland fires. Using one summer season of data from Florida, Goodrick et al. (2000) evaluated the predictive

Corresponding author address: Shiyuan Zhong, Dept. of Geography, Michigan State University, East Lansing, MI 48824.
E-mail: zhongs@msu.edu

ability of HI with regard to the potential for large wildfires and found that HI performed well in predicting large wildfires during the summer of 1998 when Florida experienced one of its most severe fire seasons on record. Other studies, however, have found that HI stays high (5 or 6) in regions with hot and dry arid climate such as regions in the western United States and southern Australia and thus does not provide warning for exceptional fire danger because of lower atmospheric instability and dryness for these regions (Long 2006; McCaw et al. 2007). Another limitation of HI is that it does not take into account wind, wind shear, and boundary layer turbulence, all of which can be important for fire behavior and fire–atmosphere interactions (Jenkins 2002; Coen et al. 2004; Clements et al. 2007, 2008). Several attempts have been made to improve the utility of HI. Heilman and Bian (2010) proposed to combine HI with turbulent kinetic energy ("HITKE") to better characterize local conditions in the atmospheric boundary layer that are important for fire behavior. Mills and McCaw (2010) proposed a continuous Haines index (C-HAINES) by analyzing atmospheric conditions for a large set of fire events over Australia for which unexpected or unusually active fire behavior was reported or large pyrocumulus clouds were observed. They found that the C-HAINES can better discriminate blow-up fires than can HI in its original form in regions with hot and dry Mediterranean or arid climate. Despite the various limitations of the original HI, it is still a component that is commonly included in fire-weather forecasts and is a useful tool that is employed by wildfire management personnel in the United States.

Previous studies have investigated regional and continental climatological characteristics of HI using observational and reanalysis data. Werth and Werth (1998) established a high-elevation HI climatological dataset for the western United States on the basis of radiosonde data for the period from 1990 to 1995. Croft et al. (2001) used radiosonde data from 1961 to 1990 to analyze the climatological characteristics of HI for the eastern United States, Alaska, Hawaii, and Puerto Rico. McCaw et al. (2007) investigated bushfire-weather climatological performance of HI in southwestern Australia using radiosonde data. Spatially consistent HI climatological results for North America that employ reanalysis datasets were produced by Winkler et al. (2007) and Lu et al. (2011). The Winkler et al. (2007) climatological dataset used the National Centers for Environmental Prediction (NCEP) global reanalysis (Kalnay et al. 1996; Kister et al. 2001) on a $2.5° \times 2.5°$ latitude and longitude grid. Lu et al. (2011) used the higher-resolution (32-km grid spacing) North American Regional Reanalysis (NARR) dataset (Mesinger et al.

2006). Although these previous climatological studies revealed spatial and temporal patterns in HI for regions of North America, they focused primarily on annual and seasonal analyses of HI. Little is known about the interannual variability of HI.

The current study can be considered as a follow-on to Lu et al. (2011) in that the same reanalysis dataset that was used to develop that climatological dataset is employed herein. The current study examines the interannual variability of HI and the spatial distribution of that variability across North America from 1979 to 2009 and explores associations between HI interannual variability and the variations of large-scale atmospheric circulations. Several studies have examined the relationship between large-scale circulation patterns and wildland fires in North America at interannual time scales. Simard et al. (1985a,b) investigated the relationship between fire activity in the United States and El Niño–Southern Oscillation (ENSO) for 1926–1982 and noticed a decrease in annual fire activity in the southern region during El Niño years but found relationships in other regions to be weak and inconsistent. In Arizona, New Mexico, and Florida, increases in area burned by wildland fire were noted during La Niña years, with the opposite occurring during El Niño years (Swetnam and Betancourt 1990; Brenner 1991). There have been suggestions that the area burned by wildland fire in some regions of North America can be correlated with the Pacific–North American (also called PNA) teleconnection pattern that occurs between the northern Pacific and North America (Johnson and Wowchuk 1993; Skinner et al. 1999; Trouet et al. 2006, 2009). Flannigan et al. (2000) found that the North Pacific oscillation (also called NPO) is associated with area burned in Canada, especially for eastern Ontario. The Pacific decadal oscillation (PDO) has also been related to fire extent in the western United States (Westerling and Swetnam 2003; Gedalof et al. 2005; Trouet et al. 2006, 2009; Taylor et al. 2008). The relations between PDO and ENSO and wildfire extent were found to be inconsistent over time (Taylor et al. 2008).

The aforementioned studies on relations between wildland fire and global climate anomalies have focused either on a specific climate phenomenon and/or on fire activity in a specific region of the United States or Canada. The current study examines the interannual variability of HI over a domain that covers most of North America and links the variability to anomalies in large-scale circulation patterns. Note, however, that a causal connection between HI and any specific type of fire behavior or seasonal fire activity has yet to be established in the peer-reviewed literature. Furthermore, continental-scale analyses of HI are complicated

TABLE 1. Calculation of the Haines index (adapted from Haines 1988). The HI depends upon static stability (factor A) and dewpoint depression (factor B) in a predefined atmospheric layer and combines the two factors into a single number: HI = factor A plus factor B.

Elev	Factor A		Factor B	
	Calculation	Categories	Calculation	Categories
Low	950-hPa temperature minus 850-hPa temperature	A = 1 if < 4°C, A = 2 if 4°–7°C, and A = 3 if ≥ 8°C	850-hPa temperature minus 850-hPa dewpoint	B = 1 if < 6°C, B = 2 if 6°–9°C, and B = 3 if ≥ °C
Middle	850-hPa temperature minus 700-hPa temperature	A = 1 if < 6°C, A = 2 if 6°–10°C, and A = 3 if ≥ 11°C	850-hPa temperature minus 850-hPa dewpoint	B = 1 if < 6°C, B = 2 if 6°–12°C, and B = 3 if ≥ 13°C
High	700-hPa temperature minus 500-hPa temperature	A = 1 if < 18°C, A = 2 if 18°–21°C, and A = 3 if ≥ 22°C	700-hPa temperature minus 700-hPa dewpoint	B = 1 if < 15°C, B = 2 if 15°–20°C, and B = 3 if ≥ 21°C

by the fact that the height above ground of the layer over which HI is calculated varies from location to location, and thus the physical processes that affect the variability of HI are not always clear (Potter 2002). Therefore this study will highlight regions in which the interannual variability in HI suggests a greater potential for erratic fire behavior or larger fire growth during time periods that coincide with elevated fire activity in the aforementioned studies.

The rest of the paper is organized as follows: Section 2 describes the method and the datasets used for the study. Results are presented in section 3, and section 4 provides a summary of the results and a discussion on the limitations and the practical implications of the study.

2. Datasets and methods

a. Datasets

Two gridded reanalysis datasets are used in this study: NARR (Mesinger et al. 2006) and its global counterpart, the reanalysis created by NCEP and the U.S. Department of Energy (DOE) (Kalnay et al. 1996; Kanamitsu et al. 2002). NARR is a long-term, dynamically consistent, high-resolution dataset for the atmosphere and land surface hydrology that was produced by NCEP using the operational NCEP regional Eta Model (Mesinger et al. 1988; Black 1988; Janjic 1994) and its data assimilation system (Rogers et al. 2001). The horizontal resolution of the NARR is 32 km, and the data are archived at 45 pressure levels and 3-hourly intervals from 1979 to the present. The gridded NARR data are used to calculate HI over North America.

To identify a relationship between HI and the variability of circulations that are larger than continental scale, a global dataset is needed. For this purpose, the NCEP–DOE Atmospheric Model Intercomparison Project (AMIP-II) reanalysis (R-2) dataset (Kanamitsu et al. 2002) is utilized, which has a horizontal resolution of T62

(~209 km), 28 vertical levels, and a temporal coverage of 4 times per day from 1 January 1979 to the present.

In addition to the two reanalysis datasets, other datasets are employed, including National Oceanic and Atmospheric Administration (NOAA) interpolated outgoing longwave radiation (OLR) data (http://www.esrl.noaa.gov/psd/data/gridded/data.interp_OLR.html) and the NOAA Extended Reconstructed Sea Surface Temperature (SST) data (http://www.esrl.noaa.gov/psd/data/gridded/data.noaa.ersst.html). The analyses also employed several indices for climate anomalies, including the Southern Oscillation index (SOI) and Niño-3.4 (http://www.cpc.ncep.noaa.gov/data/indices/), the multivariate ENSO index (MEI) (http://www.esrl.noaa.gov/psd/enso/mei/), the North Atlantic Oscillation (NAO) (http://ljp.lasg.ac.cn/dct/page/65574), and the Arctic Oscillation (AO) (http://ljp.lasg.ac.cn/dct/page/65569), as defined in Li and Wang (2003a,b).

b. Methods of analyses

The study domain spans latitudinally from 20° to 50°N and longitudinally from 50° to 130°W, which includes the contiguous United States, southern Canada, and most of Mexico. By using NARR temperature and dewpoint data at several pressure levels in the lower to midtroposphere, HI is calculated for each NARR grid point in the study domain following the procedures outlined in Table 1. To account for the variation of surface elevations across the contiguous United States, three different variants of HI were formulated on the basis of the temperature and dewpoint at 950 and 850 hPa (for low variant), 850 and 700 hPa (for midvariant), and 700 and 500 hPa (for high variant) pressure levels (Table 1). Instead of using actual elevation at a specific location to decide which HI variant is most appropriate to use, Haines (1988) employed climatological divisions and a general assessment of terrain elevation to divide the United States into three broad regions in which the use of the low-, mid-, or high-HI variant is recommended. Because the specific HI variant recommended for a region is based on the region's

general terrain elevation, a single variant may not be appropriate for a region such as the western United States that encompasses a wide range of surface elevations. An example of this is the areas along the Pacific coast that have elevations that are near sea level but would use high-variant HI according to Haines. In this study, we followed the method of Winkler et al. (2007) and used 300- and 1000-m elevation levels to determine which HI variant to use at each NARR grid point. The combined HI is then used for the domainwide analysis. The arbitrary division of the terrain elevation produces steps in HI climatological results in areas where sharp terrain gradient exists as seen in the HI climatological dataset of Winkler et al. (2007) and Lu et al. (2011). Since the analysis here considers very large spatial and temporal scale, however, the impact of this effect on the interannual variability of HI and its connection to large-scale flows, which is the focus of the study, is small.

Although the NARR data are available 8 times per day, HI is only calculated using data from 0000 UTC, the time that was originally chosen by Haines (1988) and was used by previous climatological HI studies (Winkler et al. 2007; Lu et al. 2011). Similar to these previous studies, the calculation is also limited to the period of May–October (hereinafter referred to as "warm season"), which corresponds closely to the fire season for most of the contiguous United States, especially the western United States.

The values of HI range from 2 to 6, with 2 or 3 indicating a low potential for wildfires to become erratic because of the atmospheric environment and a 6 indicating a very high chance (Haines 1988). Our analyses focus on days with moderate to high potential, or HI ≥ 4 and HI ≥ 5. The empirical orthogonal function (EOF) technique is used to identify the spatial patterns of number of days with HI ≥ 4 and HI ≥ 5. The EOF analysis can produce a set of modes that consist of spatial structures (EOFs) and corresponding time series [principal components (PCs)]. For each mode, its EOF and PC are orthogonal to the EOFs and PCs of all other modes. Each mode has a corresponding eigenvalue that describes the variance explained by the mode. In this study we analyze the first three modes that explain more than 50% of the variance. The atmospheric variables are regressed onto the PCs of the first two modes to analyze the relations between large-scale circulation patterns and spatial patterns of the two leading HI modes. The composite analysis is used to explain the spatial pattern of the third mode.

3. Results and discussions

Several previous studies (Werth and Ochoa 1993; Mills and McCaw 2010) have indicated that HI ≥ 5 or 6

are of greater importance than HI ≥ 4 for arid climate such as is found in the western United States and central and southern Australia. In regions with temperate or subtropical climate such as the southeastern United States, however, it is rare for days with HI ≥ 5 or 6 to occur. Because the domain of the current study encompasses the entire United States, the following discussion will focus more on the results for HI ≥ 4 to avoid the problem of small sample size as with HI ≥ 5 or 6 in some regions of the United States.

a. Number of days with HI ≥ 4

1) THE FIRST MODE

The spatial pattern and time series of the first EOF modes (EOF1 and PC1) of the number of days with HI ≥ 4 for the average warm season over North America are shown in Fig. 1. The first mode accounts for 22.59% of the total variance. EOF1 is positive except for small areas in the Pacific Northwest, Northeast, and Southwest of the United States and in eastern Mexico. The largest positive values appear in the southeastern United States, followed by the central plains and the Intermountain West.

The correlations between PC1 and SOI, MEI (Wolter and Timlin 1993), and Niño-3.4 are shown in Table 2. Except for May and June, PC1 is correlated significantly with all three indices, with the strongest correlation in either November (with SOI) or December (with MEI and Niño-3.4). The increase in correlation from early summer to late autumn and early winter corresponds to the development of ENSO events. During negative ENSO phase or La Niña years, a positive anomaly in the number of days with HI ≥ 4 is seen throughout most of the United States, especially in the Southeast, indicating higher HI values under the La Niña condition. In contrast, a generally negative HI anomaly appears to be associated with El Niño. Although the actual wildfire activity is, in general, much more intense in the western United States than in the southeastern or eastern United States, the effect of ENSO on HI appears to be larger in the southeastern United States. This result is consistent with findings from previous studies (Simard et al. 1985a,b; Brenner 1991; Liu 2005) in that a significant correlation between annual fire activity or area burned in regions of southern or southeastern United States and ENSO events is found at the same time that HI anomalies are correlated with ENSO.

The relation between ENSO and HI can be explored further by regressing atmospheric variables onto PC1. Figure 2 shows results from a regression of the 1000–700-hPa layer-averaged relative humidity, 850-hPa temperature, and 850-hPa wind field derived from
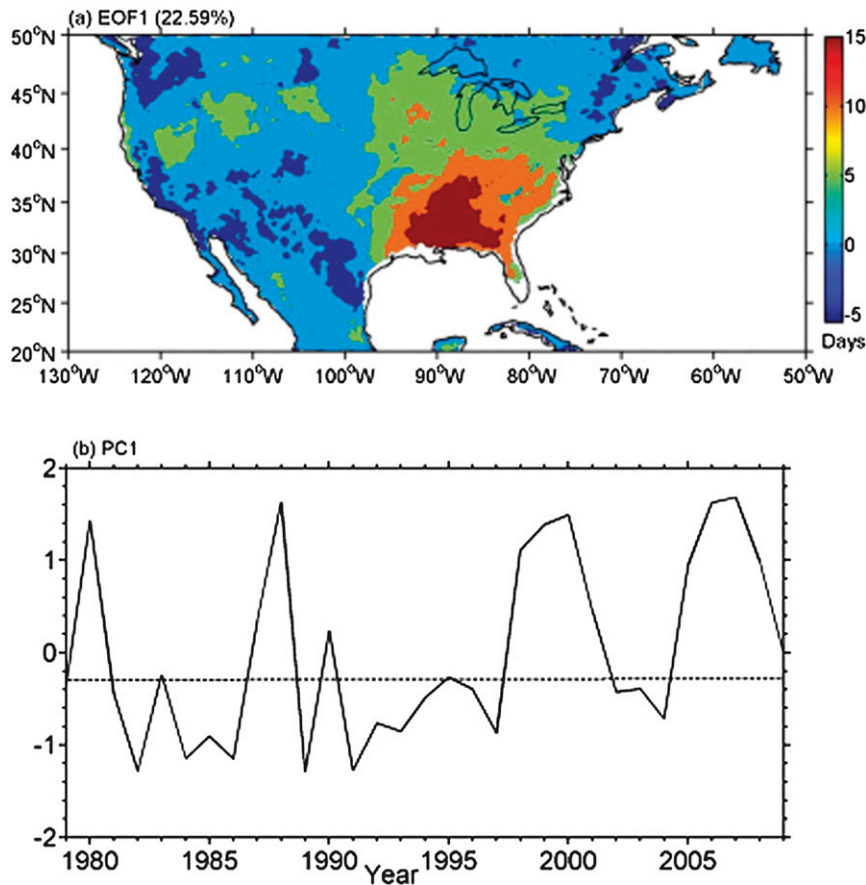
FIG. 1. (a) Spatial pattern (EOF1) and (b) time series of the coefficients (PC1) of the first mode
for the number of days with HI $\geq$ 4.

R-2 onto PC1, and Fig. 3 displays the regression of SST, 500-hPa geophysical height, and OLR onto PC1. During La Niña years (positive phase of PC1), a dry pattern occurs over most of the United States except for several small regions in the Southwest, Northwest, and Northeast (Fig. 2a). The two negative centers occur in the Southeast and Northwest, corresponding to the two positive centers of EOF1. Meanwhile a warm pattern appears over the North American continent south of 50°N (Fig. 2b). The generally dry and warm atmosphere favors a higher chance of large wildfires (Dolling et al. 2005). Figure 2c depicts an anomaly wind field that is characterized by an anomalous anticyclone over the

western and central regions of the United States and an anomalous cyclone over the eastern part of the country. Under the influence of the anticyclone, warm and dry weather prevails over the Northwest and an anomalous northerly wind between the anticyclone and cyclone brings dryer and warmer air to the Southeast, which is consistent with a larger number of days with HI $\geq$ 4. Heilman et al. (1998) also found a similar synoptic circulation pattern before the onset of fire episodes in the Southeast.

The regression of SST onto PC1 (Fig. 3a) shows a La Niña pattern with a negative SST anomaly over the tropical central and eastern Pacific Ocean and a positive

TABLE 2. Correlations between PC1 for the number of days with HI $\geq$ 4 and the ENSO indices. An asterisk indicates significance above the 95% confidence level.

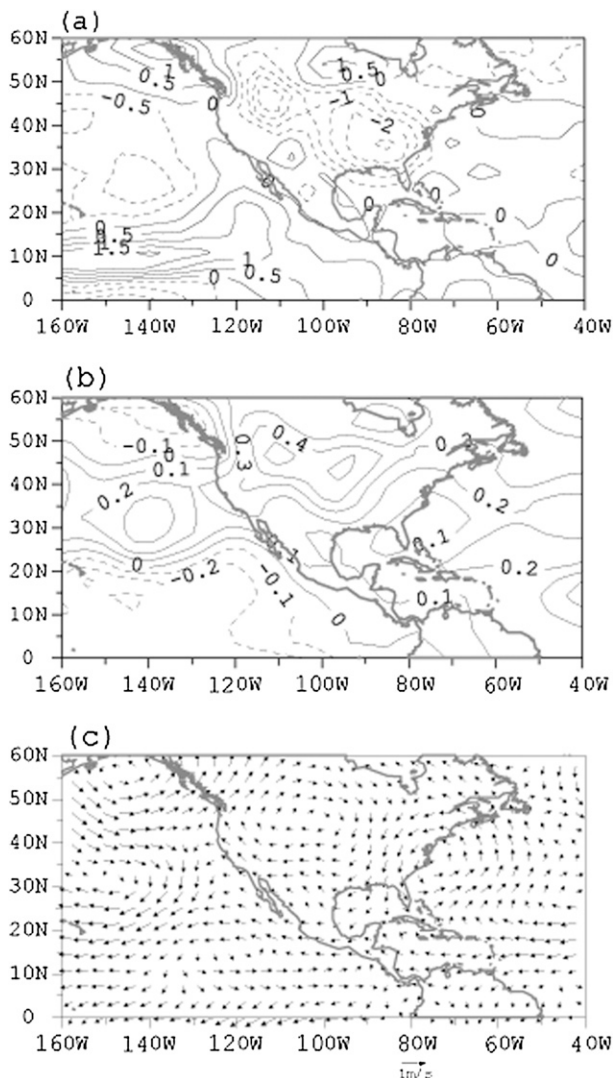| Month	1	2	3	4	5	6	7	8	9	10	11	12
SOI	0.08	−0.07	0.21	0.13	0.05	0.25	0.18	0.4*	0.45*	0.52*	0.71*	0.64*
MEI	0.07	0.03	−0.05	−0.09	−0.09	−0.29	−0.35*	−0.42*	−0.5*	−0.56*	−0.57*	−0.57*
Niño-3.4	0.03	−0.02	−0.1	−0.18	−0.29	−0.39*	−0.45*	−0.46*	−0.46*	−0.47*	−0.49*	−0.53*

FIG. 2. Regressions of (a) 1000–700-hPa layer-mean relative humidity (%), (b) 850-hPa temperature (°C), and (c) 850-hPa wind field (length of vector below 80W indicates $1 \, m \, s^{-1}$) onto the PC1.

FIG. 3. Regressions of (a) SST (°C), (b) 500-hPa geopotential height (gpm), and (c) OLR ($W \, m^{-2}$) onto the PC1. In (b), H and L indicate high and low centers, respectively.

SST anomaly over the subtropical region centered at 35°N and the tropical western Pacific Ocean. The regression of 500-hPa geopotential heights to PC1 (Fig. 3b) displays a wave-train pattern with positive anomalies over the tropical western Pacific Ocean, central Pacific Ocean (40°N, 175°W), central and western United States, and western Atlantic Ocean and negative anomalies over the tropical central Pacific Ocean (20°N, 170°W), Alaska, and the eastern United States. There is a negative anomaly of the OLR over the tropical western Pacific Ocean (Fig. 3c), where a positive SST anomaly results in convective activity and the wave train mentioned above (Fig. 3b). Trenberth et al. (1988) also found a similar wave train and used it to explain the origin of the 1988 North American drought. They showed that over the North
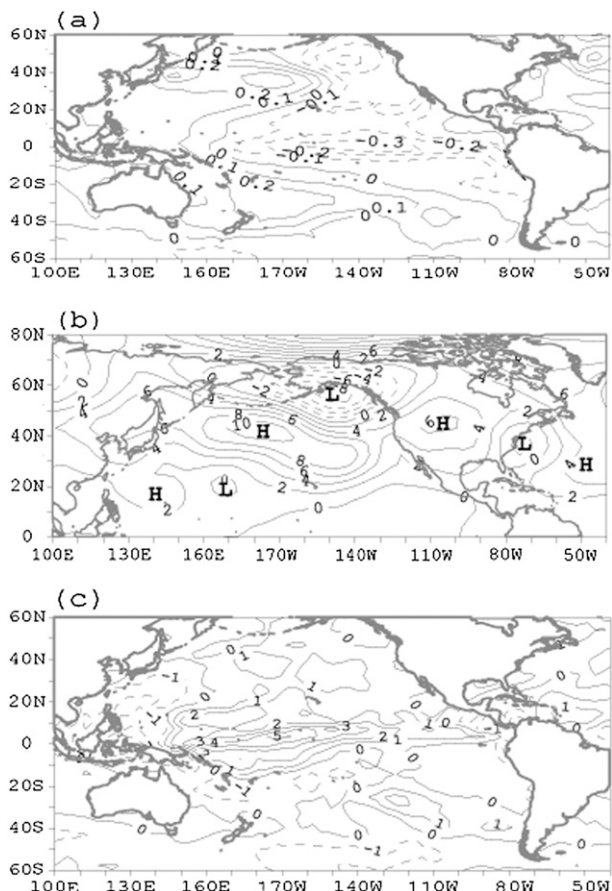
American continent drought conditions can reduce evaporation and plant transpiration, thus leading to an increase in air temperature. They also showed that besides the heating over the tropical western Pacific Ocean, the positive SST anomaly over the subtropical central North Pacific Ocean and negative SST anomaly over the tropical eastern Pacific Ocean may reinforce the wave train.

2) THE SECOND MODE

The second mode accounts for 14.40% of the total variance. Figure 4 shows the EOF2 and PC2 of the number of days with HI ≥ 4. Negative anomalies are found over the Pacific Northwest, the Intermountain West, and the north-central Great Plains of the United States. Positive anomalies occur over the southern United States and northern Mexico, with a maximum over the Southeast. The correlation between PC2 and the AO index, as defined in Li and Wang (2003b), is −0.45 for the warm season (May–October) and −0.48 for the winter season (December–February). PC2 in this
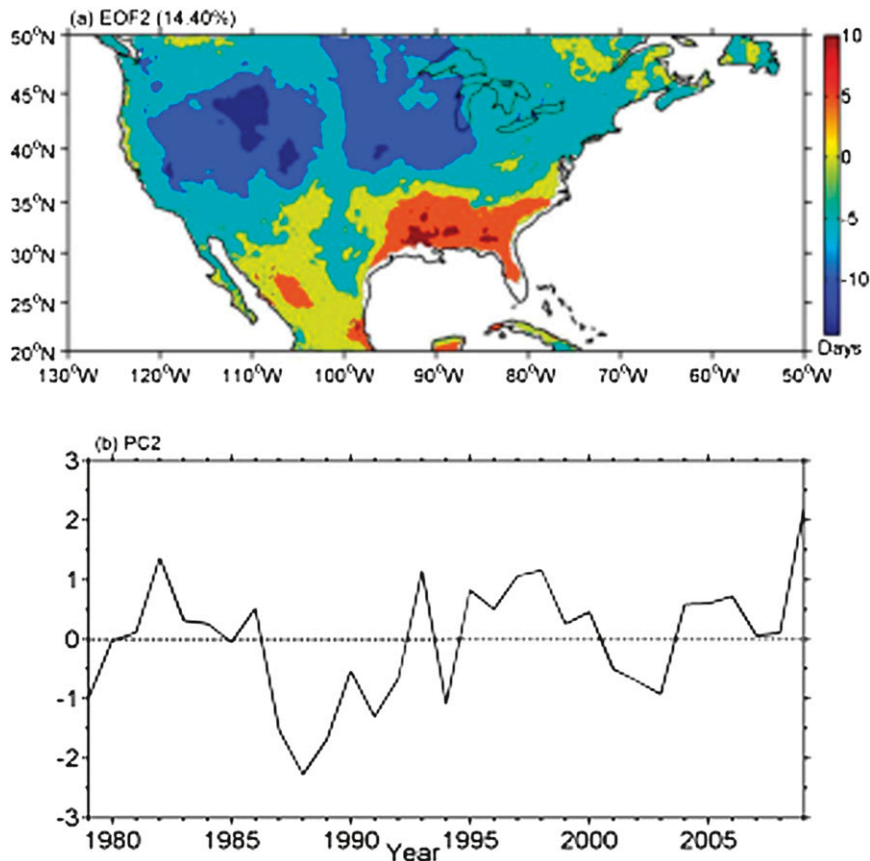
FIG. 4. (a) Spatial pattern (EOF2) and (b) time series of the coefficients (PC2) of the second
mode for the number of days with HI $\geq$ 4.

region also appears to be well correlated with the NAO index as defined in Li and Wang (2003a), with a correlation coefficient of -0.45 in northern winter and -0.48 in northern summer (June–August).

The regression of 500-hPa geopotential heights onto PC2 demonstrates the annular structure of the negative phase of the AO (Fig. 5). The midlatitude regions show four troughs located over the western United States, the North Atlantic Ocean, the northern part of the Euro-Asian continent, and the central North Pacific Ocean. A strong ridge is situated over the North Pole, and two other ridges are located over the Aleutian Islands and Baffin Island. The trough over the western United States promotes convective activity and rainfall, which leads to wet and cool weather over the region (Figs. 6a,b) and a lower number of high-HI days. The northwesterly wind from an anticyclone over the eastern Pacific Ocean brings wet and cool air to the western United States, reducing the number of days with high HI in the region (Fig. 6c). The northeasterly wind from eastern Canada and the easterly wind from the trough over the western United States provide dry weather in portions of the

northwestern and northeastern United States, which contributes to the number of days with high HI values. The anticyclone over the southeastern United States and the Gulf of Mexico blocks the northward transport of moisture from the Gulf of Mexico to the southeastern United States, but the southeasterly winds on the west side of the anticyclone help to transport Gulf moisture to western Texas. The dry and hot continental flow over most of Mexico (Fig. 6c) is responsible for the large number of days with high HI there (Fig. 4).

3) THE THIRD MODE

The spatial pattern of EOF3, which accounts for 12.76% of the total variance, shows positive anomalies over regions in the southwestern United States and over Mexico, with the largest positive anomaly center in southeastern Mexico (Fig. 7a). The negative anomalies lie over the north-central and southeastern United States. The third mode shows an interdecadal variation with PC3 values that are mostly negative before the early 1990s and mostly positive after that (Fig. 7b). On the basis of the Mann–Kendall (MK; Mann 1945) abrupt-change test, an
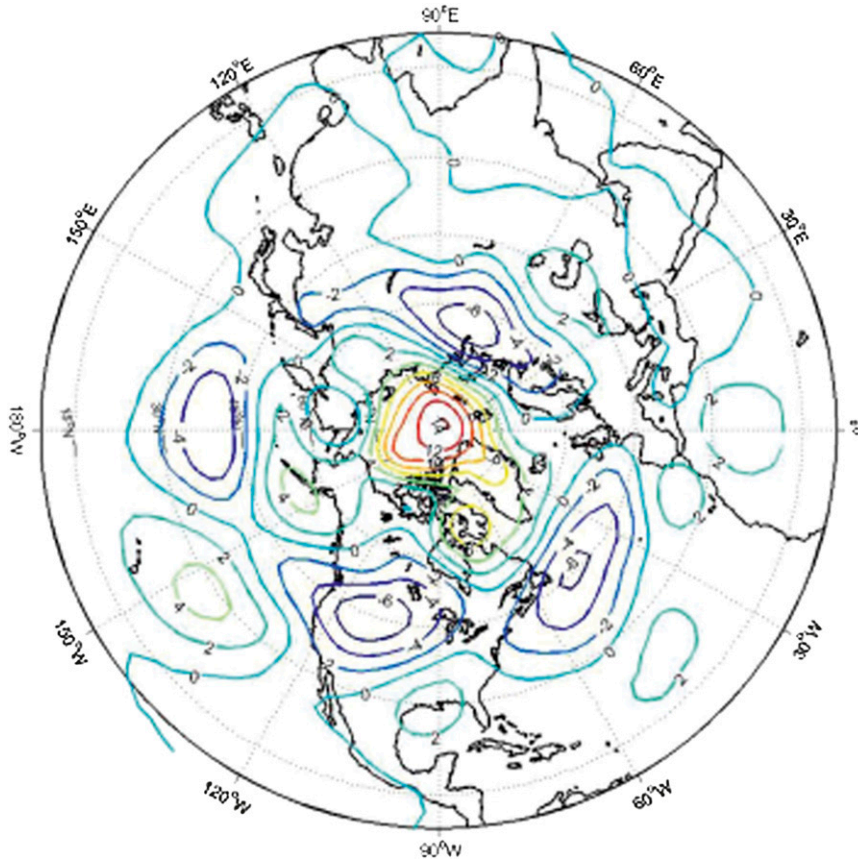
FIG. 5. Regressions of 500-hPa geopotential height (gpm) onto PC2.

abrupt changepoint occurred in 1992/93 where the two curves in Fig. 7c intersect. Corresponding to this abrupt change, the regions of positive (negative) EOF3 values in Fig. 7a indicate a larger (smaller) number of days for which HI ≥ 4 after 1992/93, whereas the opposite is true prior to that.

To explore the cause for the abrupt change in 1992/93, a composite analysis was performed in which composite maps were made separately for positive-phase years and for negative-phase years. For this analysis, positive-phase years were selected as 1994–2009 and negative-phase years were selected as 1980–90. The differences were obtained by using the mean patterns for positive-phase years minus the mean patterns for negative-phase years.

Figure 8 shows the difference maps for the 850-hPa temperature and wind fields and the 1000–700-hPa layer-mean relative humidity. Relative to the negative-phase years, the positive-phase years are characterized by a general wet anomalous pattern that occurs over south-central Canada and over the north-central and northeastern regions of the United States, with the largest anomaly over the northern plains corresponding to the negative

EOF3 anomaly over this region (Fig. 8a). The positive-phase years are also characterized by very dry anomalous conditions over the southwestern region of United States and over western Mexico that, together with significantly warmer conditions in these areas (Fig. 8b), increase the number of days with high HI. In the southeastern United States, warm and wet anomalous conditions also occur, although the confidence level is below 95% (Figs. 8a,b). The northerly wind anomaly over the western United States brings the dry and warm air to the southwestern United States and Mexico, which results in more days with HI ≥ 4 (Fig. 8c). Meanwhile the northerly wind anomaly converges with the wet and warm flow anomaly from the Gulf of Mexico in the southeastern United States, resulting in wetter conditions in the southeastern United States and a reduction in the number of days with high HI. The wetter and cooler conditions in the north-central United States during the positive-phase years relative to the negative-phase years are associated with a cyclonic cell in this region (Fig. 8c).

Figure 9 shows the difference maps (positive-phase years minus negative-phase years) for SST, 500-hPa geopotential height, and ORL. The composite result of
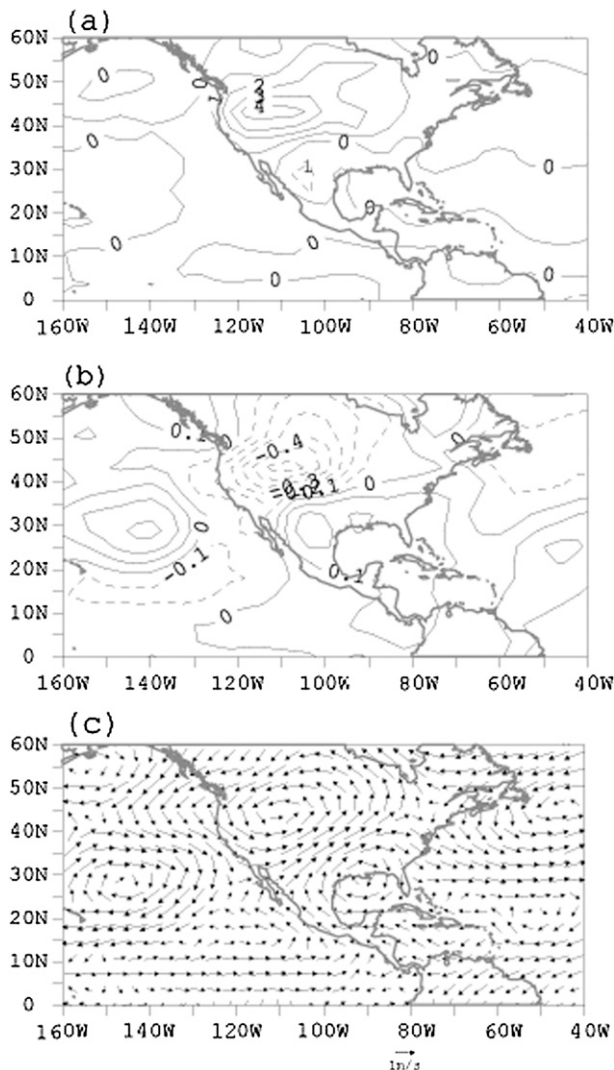
FIG. 6. As in Fig. 2, but for PC2.

SST shows a similar La Niña pattern with a significant warm anomaly over the tropical western Pacific Ocean and the southern and northern subtropical central Pacific Ocean (Fig. 9a). There is also an increase in SST across the entire North Atlantic Ocean. The warm SST anomaly over the tropical western Pacific Ocean during the positive-phase years produces convective activity (Fig. 9c) and a Rossby wave train (Fig. 9b) extending from the western Pacific Ocean to the Atlantic Ocean. The high centers of the wave train include the tropical western Pacific Ocean, the subtropical eastern Pacific Ocean, northeastern Canada, and the subtropical Atlantic Ocean. The low centers are located over the subtropical central Pacific Ocean, central North America, and the northern Atlantic Ocean. The high over the subtropical eastern Pacific Ocean leads to northerly winds over the western United States and dry

and warm conditions over the southwestern United States and western Mexico. The high over the subtropical Atlantic Ocean helps to transport moisture into the southeastern United States, leading to wet conditions in this region.

b. Number of days with HI ≥ 5

Analyses are also performed for the number of days with HI ≥ 5, a stronger indication of the potential for an existing fire to exhibit erratic fire behavior or to grow large. The EOFs and PCs of the first three modes are shown in Fig. 10. The EOF1 pattern in Fig. 10 is similar to the EOF1 pattern for HI ≥ 4 in Fig. 1, but relative to the EOF1 pattern in Fig. 1 the positive center in the eastern United States in Fig. 10 is located farther north and the positive center in the western United States is more significant. Like the EOF1 pattern for HI ≥ 4, the EOF1 pattern for HI ≥ 5 is related to ENSO. The correlation coefficients for HI ≥ 5, listed in Table 3, are very similar to the correlation coefficients for HI ≥ 4, with slightly higher correlations in May, June, and July.

The EOF2 pattern for the number of days with HI ≥ 5 exhibits positive anomalies over the southeastern United States and eastern Mexico. Its time series (PC2) is correlated significantly with the AO or the NAO during the spring season, with a correlation coefficient of −0.42. The PC1s of the number of days characterized by HI ≥ 4 and HI ≥ 5 are closely related to each other, with a correlation coefficient of 0.90. The correlation for PC2 of the number of days with HI ≥ 4 and HI ≥ 5 is somewhat lower at 0.59. Although the EOF1 and EOF2 patterns for days with HI ≥ 4 and HI ≥ 5 exhibit some small differences, they are linked to similar large-scale circulation patterns. The EOF3 pattern of the number of days when HI ≥ 5 also exhibits an interdecadal variation, with an abrupt changepoint at 1994/95. The EOF3 pattern shows variations in the western and eastern United States that are opposite to those of the central United States. The different EOF3 in the central and eastern United States may result from the large difference in the number of days with HI ≥ 4 versus HI ≥ 5 in those two regions. The composite analysis (1995–2009 minus 1979–94) reveals that the similar change in SST over the Pacific Ocean induces the abrupt change in mode 3 for HI ≥ 5.

Regression and composite analyses similar to those for HI ≥ 4 were performed. The results (not shown) indicate that the influence factors and mechanisms for HI ≥ 5 are similar to those for HI ≥ 4.

4. Summary

In this study, EOF analyses are used to investigate the interannual variability of the numbers of days with HI ≥ 4
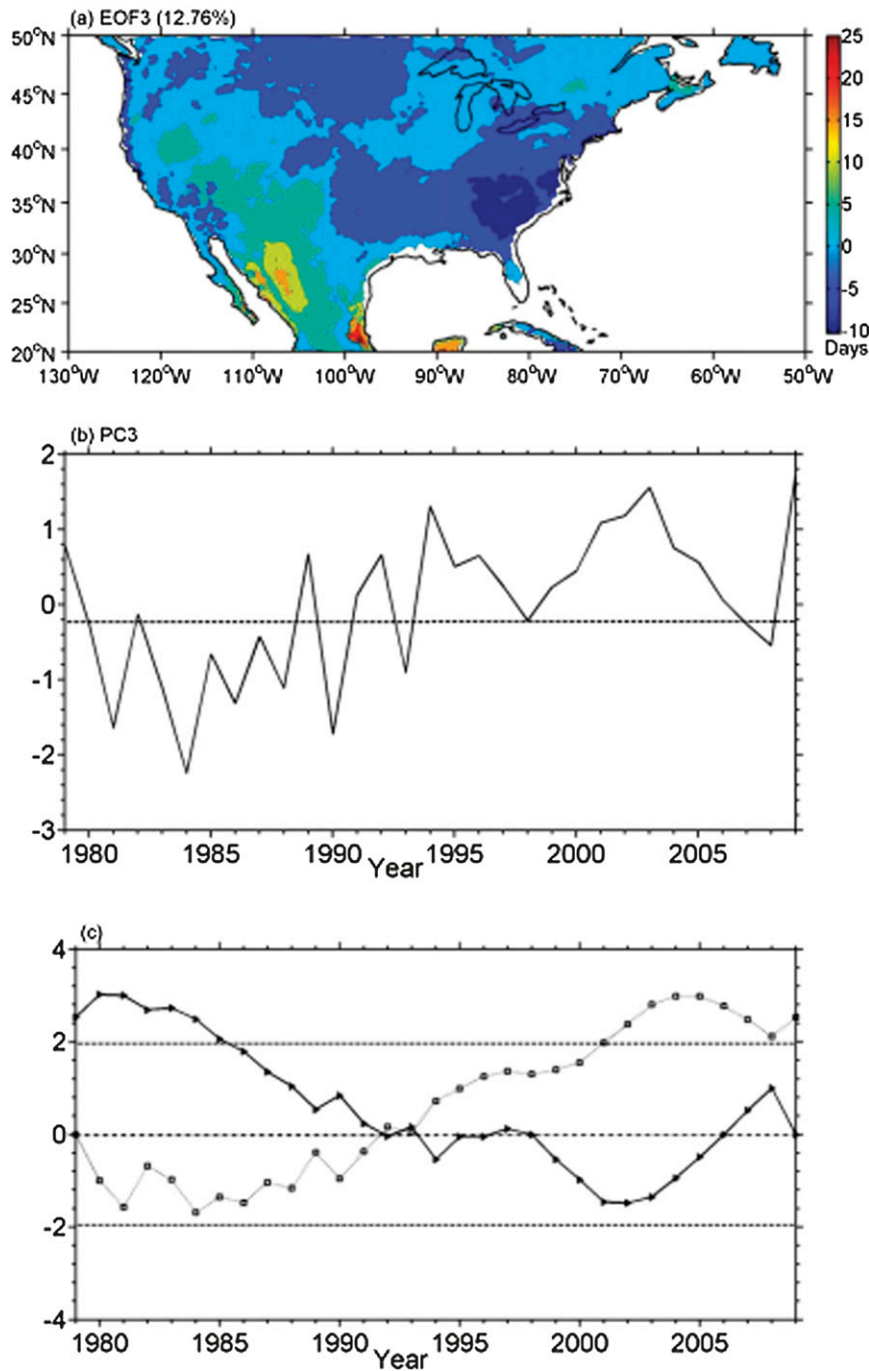
FIG. 7. (a) Spatial pattern (EOF3) and, (b) time series of the coefficients (PC3) of the third
mode of the number of days with HI ≥ 4, and (c) MK abrupt-change testing.

and HI ≥ 5 during the North American warm season
(May–October). The analyses identified three main im-
pact factors (ENSO, AO, and SST change over the Pacific
Ocean) at the interannual time scale and explored their
influence mechanisms.

The first mode of the number of days with HI ≥ 4 and
HI ≥ 5 is closely related to ENSO. During La Niña

years, the warm SST over the tropical western Pacific
Ocean induces a Rossby wave train that leads to an
anomalous high (low) pressure center over the western
(eastern) United States. The anticyclonic flow results in
warm and dry conditions in the western United States,
while the northerly winds between the high and low
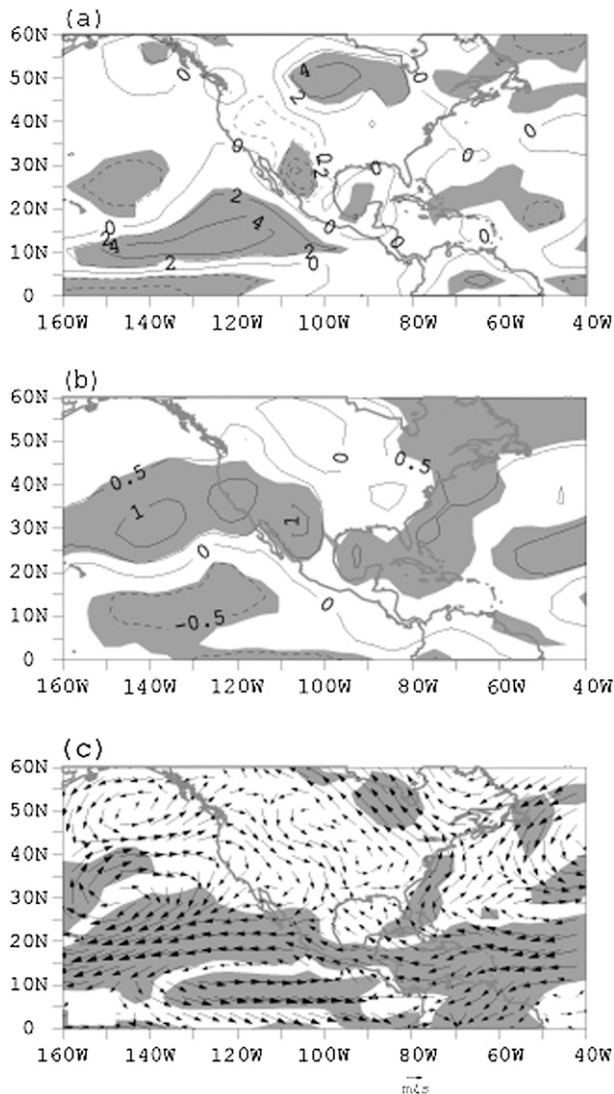bring dry air to the eastern and southeastern United

FIG. 8. Composite analyses (positive minus negative phase) of (a) 1000–700-hPa layer-mean relative humidity (%), (b) 850-hPa temperature (°C), and (c) 850-hPa wind field. The shaded regions indicate regions with >95% confidence level.

FIG. 9. Composite analyses (positive minus negative phase) of (a) SST (°C), (b) 500-hPa geopotential height (gpm), and (c) OLR (W m^{-2}). The shaded regions indicate the regions with >95% confidence level. In (b), H and L indicate high and low centers, respectively.

States. Hence, during La Niña years, there are more days for which HI ≥ 4 or 5 across the United States, especially in the western and southeastern regions. The opposite happens during El Niño years.

The second mode for the number of days on which HI ≥ 4 and HI ≥ 5 is associated with the AO. During the negative phase of the AO, an anomalous low occurs over the western United States and an anomalous high appears over the southeastern United States and Mexico. The anomalous low results in cool and wet weather and fewer days with high HI in the central and western United States. The moisture from the eastern Pacific Ocean further strengthens the wet conditions in those
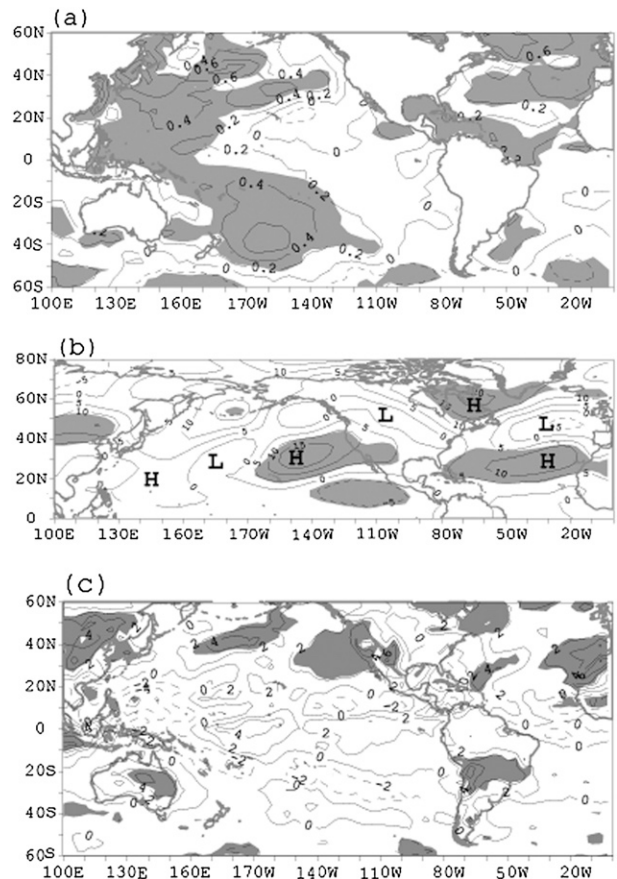
regions. The high blocks the northward transport of moisture from the Gulf of Mexico to the southeastern United States and leads to a warm and dry pattern and an increase in the number of days with high HI in the southeastern United States and western Mexico. The pattern is reversed during the positive phase of the AO.

The third mode is an interdecadal-variation mode. Starting from the early 1990s, the warm anomalous SSTs over the tropical western Pacific Ocean induce a Rossby wave train, which strengthens the subtropical eastern Pacific high and Bermuda high. The former leads to warm and dry weather in the southwestern United States and western Mexico. The latter helps to transport Gulf moisture to the southeastern United States. The opposite had occurred prior to the early 1990s.

From 1979 to 2009, the relationship between ENSO and AO and the number of days with HI ≥ 4 and HI ≥ 5 is significant. Because of the interdecadal variation of climate, however, this relationship may not be stable.
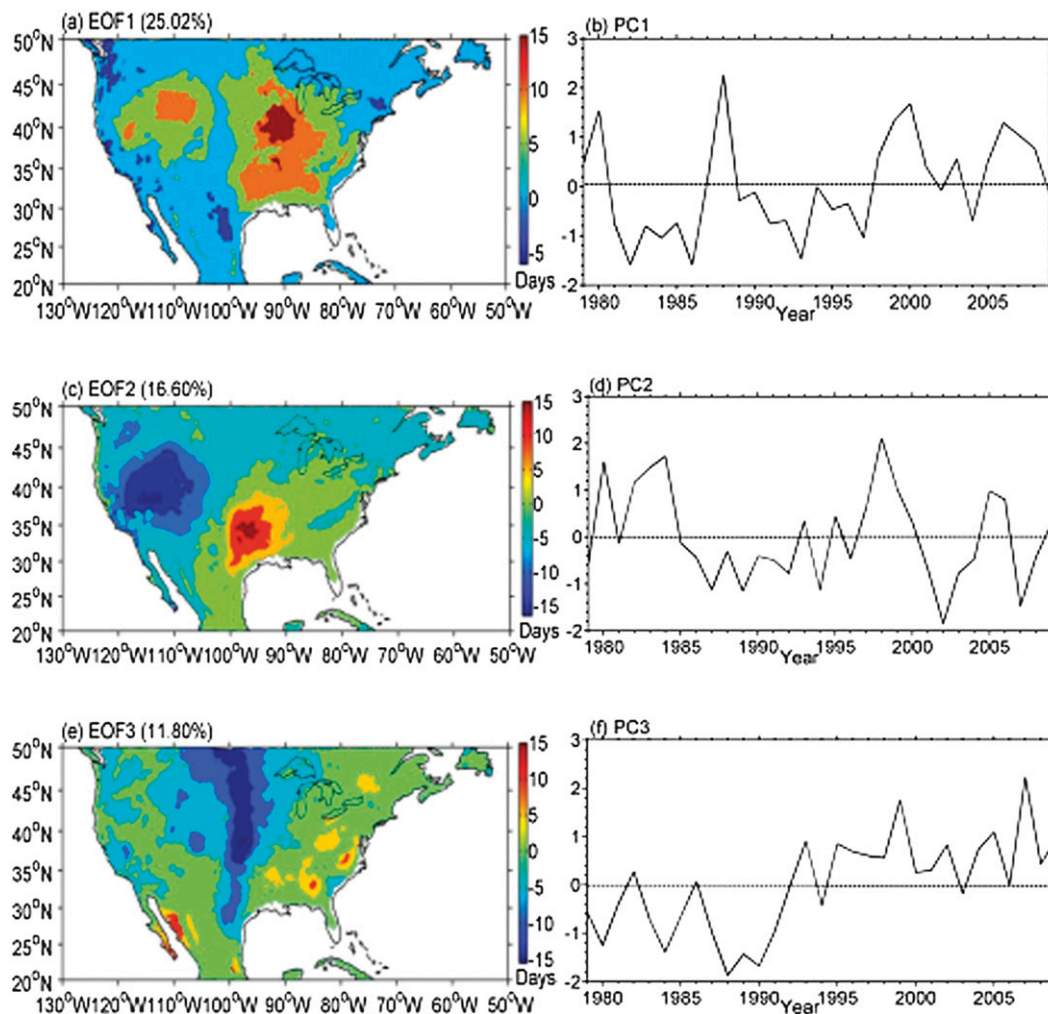
FIG. 10. (a),(c),(e) Spatial pattern (EOFs) and (b),(d),(f) time series of the coefficients (PCs) of the first three modes for the number of days with HI ≥ 5.

Taylor et al. (2008) found that the relationship between ENSO and PDO and fire extent was not stable from 1700 to 1900. Fire extent was related to PDO during the period of 1805–55 but was related to ENSO from 1700 to 1800. A study of the relations between ENSO and AO and the numbers of days with higher HI values needs to take climate change into account. An atmospheric model should also be used to examine the influence mechanisms of ENSO and AO on the number of days with high HI values.

The statistical analyses applied to the occurrence of high HI values provide new insight into the dominant large-scale circulation, temperature, and moisture patterns associated with fire weather in the United States. This insight can be used for developing seasonal predictions of fire weather in the United States because precursors of a developing anomalous circulation pattern are usually evident several months before its onset. As one of many fire-weather indices, HI is an indicator of the potential for dry, low-static-stability air in the lower

TABLE 3. Correlations between PC1 for the number of days with HI ≥ 5 and the ENSO indices. An asterisk indicates significance above the 95% confidence level.

Month	1	2	3	4	5	6	7	8	9	10	11	12
SOI	0.17	0.1	0.29	0.23	0.12	0.22	0.3	0.43*	0.47*	0.53*	0.71*	0.59*
MEI	0.00	−0.08	−0.18	−0.21	−0.25	−0.43*	−0.48*	−0.51*	−0.54*	−0.56*	−0.55*	−0.54*
Niño-3.4	−0.06	−0.1	−0.19	−0.28	−0.4*	−0.49*	−0.5*	−0.47*	−0.46*	−0.46*	−0.47*	−0.5*

atmosphere to contribute to erratic fire behavior or large fire growth, but it does not provide information on any specific type of fire behavior or seasonal fire activity. More studies involving other indices or actual fire activity data are necessary to understand fully the impact of climate on fire behavior.

REFERENCES

Bally, J., 1995: The Haines index as a predictor of fire activity in Tasmania. *Proc. Bushfire '95: Australian Bushfire Conf.,* Hobart, Tasmania, Australia, Parks and Wildlife Service, 22 pp.

Black, T. L., 1988: *The Step-Mountain, Eta Coordinate Regional Model: A Documentation.* National Oceanic and Atmospheric Administration/National Weather Service, 94 pp. [Available from NOAA Environmental Modeling Center, Rm. 207, 5200 Auth Rd., Camp Springs, MD 20746.]

Brenner, J., 1991: Southern Oscillation anomalies and their relationship to wildfire activity in Florida. *Int. J. Wildland Fire,* **1,** 73–78.

Clements, C. B., and Coauthors, 2007: Observing the dynamics of wildland grass fires: FireFlux—A field validation experiment. *Bull. Amer. Meteor. Soc.,* **88,** 1369–1382.

——, S. Zhong, X. Bian, W. E. Heilman, and D. W. Byun, 2008: First observations of turbulence generated by grass fires. *J. Geophys. Res.,* **113,** D22102, doi:10.1029/2008JD010014.

Coen, J., S. Mahalingam, and J. Daily, 2004: Infrared imagery of crown-fire dynamics during FROSTFIRE. *J. Appl. Meteor.,* **43,** 1241–1259.

Croft, P. J., M. Watts, B. E. Potter, and A. Reed, 2001: The analysis of the Haines index climatology for the eastern United States, Alaska, Hawaii, and Puerto Rico. Preprints, *Fourth Symp. on Fire and Forest Meteorology,* Reno, NV, Amer. Meteor. Soc., 8.7. [Available online at https://ams.confex.com/ams/pdfpapers/25687.pdf.]

Dolling, K., P.-S. Chu, and F. Fujioka, 2005: A climatological study of the Keetch/Byram drought index and fire activity in the Hawaiian Islands. *Agric. For. Meteor.,* **133,** 17–27.

Flannigan, M. D., B. Todd, M. Wotton, W. R. Skinner, B. J. Stocks, and D. L. Martell, 2000: Pacific sea surface temperatures and their relation to area burned in Canada. Preprints, *Third Symp. on Fire and Forest Meteorology,* Long Beach, CA, Amer. Meteor. Soc., 7.8. [Available online at https://ams.confex.com/ams/annual2000/webprogram/Paper143.html.]

Gedalof, Z., D. L. Peterson, and N. J. Mantua, 2005: Atmospheric, climatic and ecological controls on extreme wildfire years in the northwestern United States. *Ecol. Appl.,* **15,** 154–174.

Goodrick, S., D. Wade, J. Brenner, G. Babb, and W. Thomson, 2000: Relationship of daily fire activity to the Haines index and the Lavdas dispersion index during 1998 Florida wildfires. Florida Division of Forestry Rep., 13 pp. [Available online at http://www.floridaforestservice.com/publications/joint_fire_sciences/jfs_pdf/haines_hres.pdf.]

Haines, D. A., 1988: A lower atmosphere severity index for wildland fires. *Natl. Wea. Dig.,* **13,** 23–27.

Heilman, W. E., and X. Bian, 2010: Turbulent kinetic energy during wildfires in the north central and north-eastern United States. *Int. J. Wildland Fire,* **19,** 346–363.

——, B. E. Potter, and J. I. Zerbe, 1998: Regional climate change in the southern United States: The implications for wildfire occurrence. *The Productivity and Sustainability of Southern Forest Ecosystems in a Changing Environment,* R. A. Mickler and S. Fox, Eds., Springer-Verlag, 683–699.

Janjic, Z. I., 1994: The step-mountain Eta Coordinate Model: Further developments of the convection, viscous sublayer, and turbulence closure schemes. *Mon. Wea. Rev.,* **122,** 927–945.

Jenkins, M. A., 2002: An examination of the sensitivity of numerically simulated wildfires to low-level atmospheric stability and moisture, and the consequences for the Haines index. *Int. J. Wildland Fire,* **11,** 213–232.

Johnson, E. A., and D. R. Wowchuk, 1993: Wildfires in the southern Canadian Rocky Mountains and their relationship to mid-tropospheric anomalies. *Can. J. For. Res.,* **23,** 1213–1222.

Kalnay, E., and Coauthors, 1996: The NCEP/NCAR 40-Year Reanalysis Project. *Bull. Amer. Meteor. Soc.,* **77,** 437–471.

Kanamitsu, M., W. Ebisuzaki, J. Woollen, S.-K. Yang, J. J. Hnilo, M. Fiorino, and G. L. Potter, 2002: NCEP–DOE AMIP-II Reanalysis (R-2). *Bull. Amer. Meteor. Soc.,* **83,** 1631–1643.

Kister, R., and Coauthors, 2001: The NCEP–NCAR 50-Year Reanalysis: Monthly means CD-ROM and documentation. *Bull. Amer. Meteor. Soc.,* **82,** 247–267.

Li, J., and J. Wang, 2003a: A new North Atlantic Oscillation index and its variability. *Adv. Atmos. Sci.,* **20,** 661–676.

——, and ——, 2003b: A modified zonal index and its physical sense. *Geophys. Res. Lett.,* **30,** 1632, doi:10.1029/2003GL017441.

Liu, Y., 2005: Spatial relationships between SST and US wildfires. Preprints, *Sixth Symp. on Fire and Forest Meteorology,* Canmore, AB, Canada, Society of American Foresters, 1–6.

Long, M., 2006: A climatology of extreme fire weather days in Victoria. *Aust. Meteor. Mag.,* **55,** 3–18.

Lu, W., J. J. Charney, S. Zhong, X. Bian, and S. Liu, 2011: A North American Regional Reanalysis climatology of the Haines index. *Int. J. Wildland Fire,* **20,** 91–103.

Mann, H. B., 1945: Non-parametric test against trend. *Econometrika,* **13,** 245–259.

McCaw, L., P. Marchetti, G. Elliott, and G. Reader, 2007: Bushfire weather climatology of the Haines index in south-western Australia. *Aust. Meteor. Mag.,* **56,** 75–80.

Mesinger, F., and Coauthors, 2006: North American Regional Reanalysis. *Bull. Amer. Meteor. Soc.,* **87,** 343–360.

——, Z. I. Janjic, S. Nickovic, D. Gavrilov, and D. G. Deaven, 1988: The step-mountain coordinate-model description and performance for cases of Alpine lee cyclogenesis and for a case of an Appalachian redevelopment. *Mon. Wea. Rev.,* **116,** 1493–1518.

Mills, G. A., and L. McCaw, 2010: Atmospheric stability environments and fire weather in Australia—Extending the Haines index. Centre for Australian Weather and Climate Research Tech. Rep. 20, 158 pp. [Available online at http://www.cawcr.gov.au/publications/technicalreports/CTR_020.pdf.]

Potter, B. E., 2002: A dynamics based view of atmosphere–fire interactions. *Int. J. Wildland Fire,* **11,** 247–255.

Rogers, E., M. Ek, Y. Lin, K. Mitchell, D. Parrish, and G. DiMego, 2001: Changes to the NCEP Meso Eta analysis and forecast system: Assimilation of observed precipitation, upgrades to land surface physics, modified 3DVAR analysis. National Center for Environmental Predictions Environmental Modeling Center

Rep. [Available online at http://www.emc.ncep.noaa.gov/mmb/mmbpll/spring2001/tpb/.]

Simard, A. J., D. A. Haines, and W. A. Main, 1985a: El Niño and wildland fire: An exploratory study, in weather—The drive train connecting the solar engine to forest ecosystems. Preprints, *Eighth Conf. on Fire and Forest Meteorology,* Bethesda, MD, Society of American Foresters, 88–95.

——, ——, and ——, 1985b: Relations between El Niño/Southern Oscillation anomalies and wildland fire activity in the United States. *Agric. For. Meteor.,* **36,** 93–104.

Skinner, W. R., B. J. Stocks, D. L. Martell, B. Bonsal, and A. Shabbar, 1999: The association between circulation anomalies in the mid-troposphere and area burned by wildland fire in Canada. *Theor. Appl. Climatol.,* **63,** 89–105.

Swetnam, T. W., and J. L. Betancourt, 1990: Fire–Southern Oscillation relations in the southwestern United States. *Science,* **249,** 1017–1020.

Taylor, A. H., V. Trouet, and C. N. Skinner, 2008: Climatic influence on fire regimes in mountain forests of the southern Cascades, California, USA. *Int. J. Wildland Fire,* **17,** 60–71.

Trenberth, K. E., G. W. Branstator, and P. A. Arkin, 1988: Origins of the 1988 North American drought. *Science,* **242,** 1640–1645.

Trouet, V., A. H. Taylor, A. M. Carleton, and C. N. Skinner, 2006: Fire-climate interactions in forests of the American Pacific coast. *Geophys. Res. Lett.,* **33,** L18704, doi:10.1029/2006GL027502.

——, ——, ——, and ——, 2009: Interannual variations in fire weather, fire extent, and synoptic-scale circulation patterns in northern California and Oregon. *Theor. Appl. Climatol.,* **95,** 349–360.

Werth, J., and P. Werth, 1998: Haines index climatology for the western United States. *Fire Management Notes,* **58,** 8–17.

Werth, P., and R. Ochoa, 1993: The evaluation of Idaho wildfire growth using the Haines index. *Wea. Forecasting,* **8,** 223–234.

Westerling, A. L., and T. W. Swetnam, 2003: Interannual to decadal drought and wildfire in the western United States. *Eos, Trans. Amer. Geophys. Union,* **84,** 545–560.

Winkler, J. A., B. E. Potter, D. F. Wilhelm, R. P. Shadbolt, K. Piromsopa, and X. D. Bian, 2007: Climatological and statistical characteristics of the Haines Index for North America. *Int. J. Wildland Fire,* **16,** 139–152.

Wolter, K., and M. S. Timlin, 1993: Monitoring ENSO in COADS with a seasonally adjusted principal component index. *Proc. 17th Climate Diagnostics Workshop,* Norman, OK, NOAA/NMC/CAC, NSSL, Oklahoma Climate Survey, CIMMS and the School of Meteorology, University of Oklahoma, 52–57.